Biallelic variants in *COX18* cause a mitochondrial disorder primarily manifesting as peripheral neuropathy

Camila Armirola-Ricaurte,[1,2,†,‡] Laura Morant,[1,2,‡] Isabelle Adant,[3,4] Sherifa Ahmed Hamed,[5] Menelaos Pipis,[6,7] Stephanie Efthymiou,[6] Silvia Amor-Barris,[1,2] Derek Atkinson,[1,2,§] Liedewei Van de Vondel,[8,9] Aleksandra Tomic,[10,11] Sara Seneca,[12] Els de Vriendt,[1,2] Stephan Zuchner,[13] Bart Ghesquiere,[14,15] Michael Hanna,[6] Henry Houlden,[6] Michael P. Lunn,[6] Mary M. Reilly,[6] Vedrana Milic Rasic[10,16] and Albena Jordanova[1,2,17]

‡**These authors contributed equally to this work.**

Abstract

Defects in mitochondrial dynamics are a common cause of Charcot-Marie-Tooth disease (CMT), while primary deficiencies in the mitochondrial respiratory chain (MRC) are rare and atypical for this etiology. This study aims to report *COX18* as a novel CMT-causing gene. This gene encodes an assembly factor of mitochondrial Complex IV (CIV) that translocates the C-terminal tail of MTCO2 across the mitochondrial inner membrane.

Exome sequencing was performed in four affected individuals from three families. The patients and available family members underwent thorough neurological and electrophysiological assessment. The impact of one of the identified variants on splicing, protein levels, and mitochondrial bioenergetics was investigated in patient-derived lymphoblasts. The functionality of the mutant protein was assessed using a Proteinase K protection assay and immunoblotting. Neuronal relevance of COX18 was assessed in a *Drosophila melanogaster* knockdown model.

Exome sequencing coupled with homozygosity mapping revealed a homozygous splice variant c.435-6A>G in *COX18* in two siblings with early-onset progressive axonal sensory-motor peripheral neuropathy. By querying external databases, we identified two additional families with rare deleterious biallelic variants in *COX18*. All eight affected individuals presented with axonal CMT and some patients also exhibited central nervous system symptoms, such as dystonia and spasticity. Functional characterization of the c.435-6A>G variant demonstrated that

it leads to the expression of an alternative transcript that lacks exon 2, resulting in a stable but defective COX18 isoform. The mutant protein impairs CIV assembly and activity, leading to a reduction in mitochondrial membrane potential. Downregulation of the *COX18* homolog in *Drosophila melanogaster* displayed signs of neurodegeneration, including locomotor deficit and progressive axonal degeneration of sensory neurons.

Our study presents genetic and functional evidence that supports *COX18* as a newly identified gene candidate for autosomal recessive axonal CMT with or without central nervous system involvement. These findings emphasize the significance of peripheral neuropathy within the spectrum of primary mitochondrial disorders and the role of mitochondrial CIV in the development of CMT. Our research has important implications for the diagnostic workup of CMT patients.

Author affiliations:

1 Molecular Neurogenomics group, VIB Center for Molecular Neurology, VIB, 2610, Antwerp, Belgium

2 Molecular Neurogenomics group, Department of Biomedical Sciences, University of Antwerp, 2610 Antwerp, Belgium

3 Laboratory of Hepatology, Department of Chronic Diseases, Metabolism and Ageing, Katholieke Universiteit Leuven, 3000, Leuven, Belgium

4 Department of Pediatrics, University Hospitals Leuven, 3000, Leuven, Belgium

5 Department of Neurology and Psychiatry, Assiut University Hospitals, 2074020, Assiut, Egypt

6 Centre for Neuromuscular Diseases, Department of Neuromuscular Diseases, UCL Queen Square Institute of Neurology, WC1N 3BG, London, UK

7 Neuropathology Department and Center for Neuromuscular Disorders, The Cyprus Institute of Neurology and Genetics, 2371, Nicosia, Cyprus

8 Translational Neurosciences, Faculty of Medicine and Health Sciences, University of Antwerp, 2610, Antwerp, Belgium

9 Laboratory of Neuromuscular Pathology, Institute Born-Bunge, University of Antwerp, 2610, Antwerp, Belgium

10 Faculty of Medicine, University of Belgrade, 11000, Belgrade, Serbia

11 Neurology Clinic, University Clinical Center of Serbia, 11000, Belgrade, Serbia

12 Clinical Sciences, Research Group Reproduction and Genetics, Centre for Medical Genetics, Universitair Ziekenhuis Brussel (UZ Brussel), Vrije Universiteit Brussel (VUB), 1090, Brussels, Belgium

13 Dr. John T. Macdonald Foundation Department of Human Genetics and John P. Hussman Institute for Human Genomics, University of Miami Miller School of Medicine, Miami, FL 33136, USA

14 Metabolomics Expertise Center, Center for Cancer Biology, CCB-VIB, 3000 Leuven, Belgium

15 Metabolomics Expertise Center, Department of Oncology, Katholieke Universiteit Leuven, 3000, Leuven, Belgium

16 Clinic for Neurology and Psychiatry for Children and Youth, 11000, Belgrade, Serbia

17 Department of Medical Chemistry and Biochemistry, Medical University-Sofia, 1431, Sofia, Bulgaria

[†]Present address Exeter Centre of Excellence for Diabetes Research (EXCEED), University of Exeter Medical School, EX1 2HZ, Exeter, UK

[§]Present address: Max Planck Institute of Immunobiology and Epigenetics, 79108, Freiburg, Germany

Correspondence to: Albena Jordanova

University of Antwerp, Campus Drie Eiken, Building V, Universiteitsplein 1, 2610, Antwerp, Belgium

E-mail: albena.jordanova@uantwerpen.be

Running title: COX18 is a novel cause of axonal CMT

Keywords: cytochrome c oxidase assembly factor 18; complex IV deficiency; CMT

Introduction

Charcot-Marie-Tooth (CMT) disease refers to a group of clinically and genetically heterogeneous sensory-motor peripheral neuropathies. Together, they are the most common inherited neuromuscular disorder, with a prevalence of 9,7-82,3 patients per 100,000 individuals.[1] Over 100 genes across all patterns of inheritance have been linked to CMT.[2] Some of these genes encode proteins that participate in essential nerve-specific processes, such as axonal transport, myelination, and synaptic transmission. Others are however involved in general housekeeping pathways (e.g., endosomal trafficking, mRNA processing). It remains unclear why defects in such ubiquitous proteins predominantly affect peripheral nerves.

Mitochondrial dynamics plays a significant role in CMT.[3] Variants in *MFN2*, involved in mitochondrial fusion, are among the most prevalent causes of axonal CMT (CMT2), accounting for 21-30% of the genetically diagnosed individuals.[4,5] Similarly, pathogenic variants in *SLC25A46*, another mitochondrial fusion factor, have been linked to CMT.[6] Variants in *GDAP1*, encoding a protein implicated in mitochondrial fission, are another common cause of CMT2, specifically prevalent in certain geographic regions of the world.[7-10] Defects in these proteins impair mitochondrial trafficking, distribution, and turnover along the axons, ultimately leading to bioenergetic failure.[11,12]

Whereas mitochondrial dynamics defects are a well-established pathway in CMT, primary defects in the respiratory chain are a rare and relatively unexplored etiology. In the past decade, next-generation sequencing studies have demonstrated that defects in the components or assembly of almost every mitochondrial complex can lead to peripheral neuropathy as predominant manifestation. These include biallelic pathogenic variants in genes encoding structural subunits of Complex I (NDUFS6, NDUFA9, MT-ND3), or genes encoding subunits and assembly factors of cytochrome c oxidase (Complex IV) (*SURF1*, *COA7*, *COX6A1, COX20).*[13-22] Finally, a variant in the mitochondrial-encoded MT-ATP6, a subunit of ATP

synthase (Complex V), has been estimated to account for approximately 1% of unsolved CMT2 patients.[23]

Here, we report biallelic variants in *COX18*, cytochrome c oxidase assembly factor 18, as a novel cause of CMT2. Defects in this gene have very recently been associated with severe and rapidly progressive encephalopathy with neonatal or infantile onset and associated with cardiomyopathy, oculomotor apraxia and peripheral neuropathy.[24,25] In the current study, patients carrying deleterious variants in *COX18* exhibit as a cardinal feature progressive sensory-motor polyneuropathy of variable onset, and some of them also display signs of central nervous system (CNS) involvement. Functional studies in patient-derived lymphoblasts suggest that the underlying mechanism is a partial loss of function of COX18 that leads to reduced assembly and activity of Complex IV (CIV). Downregulation of the COX18's ortholog in *Drosophila* induces behavioral and neuropathological phenotypes common to other fly models of CMT disease.

Materials and methods

Participants

Patients underwent routine neurologic and electrophysiological examinations. This study was approved by the local institutional review boards. All patients signed an informed consent form before enrolment.

Exome sequencing and homozygosity mapping

Genomic DNA was isolated from peripheral blood mononuclear cells according to standard protocols. Exome sequencing (ES) was performed in the two affected members from family 1 using SeqCap EZ Exome Probes v3.0 kit (Roche Holding AG, Basel, Switzerland) for capture. Then, 150 bp exome paired-end sequencing was run on NextSeq 150 platform (Illumina, San Diego, CA). Sequencing read mapping, variant calling, and annotation were done using GenomeComb (version 0.98.3).[26] Homozygosity mapping based on ES data was performed using the HOMWES tool as described.[27] Variants were filtered and prioritized within the resulting regions of homozygosity based on a recessive model of inheritance with the following criteria: non-synonymous or splice variants with minor allele frequency (MAF) below 5% and no

homozygotes in the control population database gnomAD v2.1.1.[28] Prioritized variants were evaluated further using Alamut Visual Plus (Sophia Genetics, Switzerland).

Mitochondrial DNA sequencing and analysis

DNA of the proband from family 1 (1.II.1) was isolated from peripheral blood mononuclear cells and the mitochondrial DNA (mtDNA) was enriched using long range PCR. A DNA library was prepared using the NebNext kit (Bioké, Leiden, Netherlands) and 2 x 100bp pair-end sequencing was performed on a NovaSeq 6000 machine (Illumina). Additionally, the mtDNA sequencing reads from the probands of family 2 (2.II.1) and 3 (3.II.1) were derived from the ES data available. The reads were aligned to the human mitochondrial reference genome NC_012920.1. After standard quality control, variant calling and annotation, variants were annotated with MToolBox[29] and MITOMAP.[30] Haplogroup was determined with Haplogrep v2.4.0. [31] The sequencing data was analysed and interpreted based on available information in the literature and published databases, including gnomAD[28] and MITOMAP.[30]

Variant segregation and cohort screening

The resulting variants were confirmed and segregated in the available family members by Sanger sequencing as previously described.[27] A cohort of 362 CMT patients with unknown genetic diagnosis was screened for deleterious variants in *COX18* using an amplicon target amplification assay (Agilent, https://www.agilent.com). Re-sequencing was performed on a MiSeq (Illumina) platform using 250 bp pair-end reads targeting all exons and exon-intron boundaries of the canonical *COX18* transcripts. The primers used are listed in the Supplementary Table 1. All additional variants identified in the cohort screening were validated by Sanger sequencing. Furthermore, GENESIS[32] and RD-Connect Genome-Phenome Analysis Platform (GPAP) (https://platform.rd-connect.eu/)[33] were queried online to find additional unrelated CMT patients with *COX18* candidate variants. In this way two additional COX18 families were identified (family 2 via GPAP, family 3 via GENESIS).

Cell culture

Peripheral blood mononuclear cells from the patients and parents of family 1 were isolated and transformed with Epstein-Barr virus (EBV) as described.[34]

RNA extraction, cDNA synthesis and RT-qPCR

Total RNA was extracted from the lymphoblasts using the Universal RNA Purification kit (Roboklon, Berlin, Germany), followed by DNAse treatment with TURBO DNA-free kit (Invitrogen, Thermo Fisher Scientific, Waltham, MA, USA). cDNA was synthesized using iScript Advanced cDNA synthesis kit for RT-qPCR (Bio-Rad, Hercules, CA, USA). *COX18* cDNA was amplified using the primers listed in Supplementary Table 1. *COX18* transcripts of interest were amplified using the Power SYBR green PCR master mix (Applied Biosystems, Waltham, MA, USA) and the fluorescence was measured in the the QuantStudio™ 6 Flex Real-Time PCR System (Thermo Fisher Scientific). Gene expression levels were measured using Qbase+ software (Biogazelle, Gent, Belgium). Five different housekeeping genes (*GAPDH,SDHA,TBP,HPRT1,HMBS*) were included in the analysis to normalize the data across the samples. The primers used for RT-qPCR are listed in Supplementary Table 1.

Targeted cDNA long-read sequencing

Targeted long-read sequencing (T-LRS) of *COX18* cDNA was performed on a MinION platform using a Flongle adapter (Oxford Nanopore technologies - ONT, Oxford, UK) as described.[35] For this purpose, a primer pair was designed to anneal on exon 1 and 4, flanking all previously known splicing events of *COX18*. As *COX18* is expressed at low levels in most tissues, PCR amplification with 35 cycles was performed. Sequencing reads were aligned to human genome assembly 38 with minimap2 v5.0.11 in spliced alignment mode. Read splice junction correction, high-confidence isoform definition, and quantification were performed using FLAIR v1.5.[36]

Mitochondrial isolation

Lymphoblasts were collected from one T175 flask per individual, washed with PBS, and resuspended in mitochondrial isolation buffer (250mM mannitol, 0.5mM EGTA, 5 mM HEPES/KOH, pH 7.4). The cells were lysed using 10 strokes of a 1 ml syringe attached to a 26.5G needle. The mitochondrial fractions were isolated by differential centrifugation as described.[37]

Proteinase K protection assay

Proteinase K protection assay was conducted as described.[37] Mitochondria were divided equally into four tubes; two were resuspended in mitochondrial isolation buffer and two in osmotic swelling buffer without mannitol (0.5mM EGTA, 5 mM HEPES/KOH, pH 7.4) to generate mitoplasts. One tube from each condition was treated with 5µg/ml of Proteinase K (Thermo Fisher Scientific) for 20 min at 4°C. Digestion was inhibited by incubation with 1mM phenylmethylsulfonyl fluoride solution (PMSF, sc-482875, Santa Cruz Biotechnology) for 10 min on ice. Mitochondria and mitoplasts were isolated by centrifugation (10,000 g, 10 min, 4°C), resuspended in Laemmli buffer, boiled for 5 min, and immunoblotted as explained below.

Complex IV enzymatic assay

Complex IV activity was measured in mitochondrial fractions as previously described.[38] Lymphoblast pellets were obtained from one T175 flask and resuspended in 1ml ice-cold Mega Fb buffer (250 mM sucrose, 2 mM HEPES, 0.1 mM EGTA, pH 7.4) supplemented with 0.08 mM digitonin. The cells were disrupted on an ice slurry with 20 strokes of a Teflon-glass Wheaton homogenizer driven by a Glas-Col High Speed Homogenizer variable speed bench top drill at 1800 rpm. Mitochondrial fractions were isolated by differential centrifugation as described.[37] The resulting pellet was resuspended in ice-cold hypotonic buffer (25 mM potassium phosphate, pH 7.2, 5 mM $MgCl_2$) and subjected to three freeze-thaw cycles in dry ice and ethanol slurry. CIV and citrate synthase (CS) activity was measured in a Cary 300 UV-Vis spectrophotometer (model number G9823A) as previously described.[39] Before measurements, reaction cuvettes with 50mM KPi (pH 7.4) were equilibrated to 30°C. Each enriched mitochondria sample was added, followed by the addition of reduced cytochrome c to a concentration of 15mM. After briefly mixing, the absorbance was immediately measured. Then, $K_3Fe(CN)_6$ was added to 1mM to achieve complete oxidation of cytochrome c, and a final reading was taken. The results were calculated as described.[39]

Measurement of mitochondrial membrane potential

Lymphoblasts were washed twice with prewarmed phosphate-buffered saline (PBS) and incubated with 20uM TMRE (ENZ-52309, Tetramethylrhodamine ethyl ester perchrolate, Enzo Life Sciences, Exeter, UK) for 30 minutes at 37°C. Positive control cells were incubated with 20

nM FCCP (ab120081, Abcam) for 5 minutes at 37°C before staining. After staining, cells were rinsed with prewarmed PBS and analyzed with flow cytometry on MACSQuant Analyzer 10 (Miltenyi Biotec, Bergisch Gladbach, Germany). Median fluorescence intensity (MFI) was measured using FlowLogic 8.6 software (Inivai Technologies, Mentone, Australia).

Western blotting

Total protein or mitochondrial fractions from lymphoblasts were lysed, separated by SDS-PAGE, and transferred to blotting membranes as described.[34] Membranes were incubated with the following primary antibodies: anti-COX18 (Protein atlas, HPA049489, 1:1000), anti-MTCO2 (Abcam, ab913117, 1:1000), anti- αTubulin (Abcam, ab7291, 1:5000), anti-VDAC1 (Abcam, ab14734,1:1000), anti-SDHA (Genetex, GTX632636, 1:3000) anti-HCCS (Proteintech, 15118-1-AP, 1:2000), OXPHOS Human WB Antibody cocktail (Abcam, ab110411, 1:200), anti-ATP5C1 (ThermoFisher Scientific, 60284-1-IG, 1:1000). Anti-rabbit IgG (Promega, W401B, 1:10000), anti-mouse IgG1 and IgG2b (Southern Biotech, 1070-05, 1090-05, 1:10000) were used as secondary antibodies. The blots were developed with Pierce ECL Plus substrate (Thermo Fisher Scientific) and imaged using the Amersham Imager 600 (GE Healthcare, Wauwatosa, WI, USA). Images were analyzed using ImageJ[40] to calculate the mean pixel gray values of each band.

Drosophila stocks and maintenance

The following fly stocks were obtained from the Bloomington Drosophila Stock Center (Bloomington, IN, USA): UAS-mCD8.ChRFP (BL27391), dpr-Gal4 (BL25083), Mi{MIC}CG4942^{MI03165} (dCOX18^{MI03165}, BL36211). The RNAi lines for dCOX18 (dCOX18-RNAi, CG4942^{GD2380}, v42888) and Sply (RNAi Sply, Sply^{HMS02526}, v42834) were obtained from Vienna Drosophila Resource Center (Vienna, Austria). The UAS-YARS1 fly line expressing human YARS1 with a CMT-causing variant (YARS1-E196K) was generated and described previously.[41] The nsyb-Gal4 driver line was kindly provided by M. Leyssen and B. Dickson.[42] All crosses were performed at 25°C, 12h light/dark cycle, on Nutri-Fly™ flood (Flystuff; San Diego, USA).

Fly RNA extraction, cDNA synthesis, and RT-qPCR

Total RNA was isolated from the heads of adult flies following standard Trizol (Qiagen, Hilden, Germany) and chloroform extraction protocol. RNA was treated with TURBO DNA-free kit (Invitrogen, Thermo Fisher Scientific, Waltham, MA, USA) followed by cDNA synthesis using iScript Advanced cDNA synthesis kit for RT-qPCR (Bio-Rad). To confirm the downregulation of *COX18*'s ortholog, dCOX18 (CG4942), in the heterozygous dCOX18^{MI03165} fly line, gene expression levels were determined by quantitative RT-PCR using SYBR green PCR master mix (Applied Biosystems) and compared to Nsyb-Gal4-driven dCOX18 pan-neuronal knockdown using RNAi (Nsyb-GAL4 > dCOX18-RNAi) and a control *yw* fly line. The following targets were used as housekeeping genes: Gapdh1, RpL32, RpS13, Act42A, Act79B. The housekeeping gene with the most stable expression across samples was used to normalize the data. The results were analyzed using the qBase+ software. The primers used for RT-qPCR are described in Supplementary Table 1.

Wing degeneration assay

A *Drosophila* wing degeneration assay was performed as described previously.[43] Flies carrying the UAS-mCD8ChRFP construct in their genome were crossed with flies with the dpr-Gal4 driver to express the mChrerry protein in the chemosensory neurons of the wing margin bristles. The construct encodes a membrane-bound RFP-labeled mCherry protein that is incorporated into the neuronal membrane. When the flies reached the desired age (1 day or 30 days post eclosion), one wing per fly was clipped as close as possible to the thorax. Each wing was washed with PBS supplemented with 0,2% Triton X-100 and then mounted in Dako mounting medium (Agilent technologies, Santa Clara, CA USA). Axonal degeneration was determined by visual inspection of the fragmentation of the neuronal membrane and the proportion of wings depicting the fragmented phenotype per fly line was calculated.

Negative Geotaxis Assay

The effect of dCOX18 downregulation on fly locomotion was studied using a negative geotaxis assay as described.[44] From each fly line, 10 days post eclosion female flies with clipped wings were placed in a closed vial of 49 mm diameter. Fly movements were recorded using an infrared camera. After acclimation for 1 hour, the flies were tapped onto the bottom of the vial using a

semi-automated FlyCrawler device (Peira Scientific Instruments, Beerse, Belgium). For each genotype, 10 groups of 10 flies were tested at least 15 times and the average time taken by the 10 fastest flies to reach a mark at a height of 82 mm was calculated.

Statistical analyses

GraphPad Prism 9.2.0 was used for statistical analyses. The test for each experimental measurement is reported within the figure legends. Briefly, continuous variables were compared with a two-tailed Student's t-test or a one-way ANOVA followed by Tukey's multiple-comparison test. Categorical variables were analyzed by pairwise comparison with a one-sided Chi-square test. In all figures p-values are reported as * $P< 0.05$, ** $P<0.01$, *** $P<0.001$, **** $P<0.0001$, and *ns* for non-significant.

Results

Exome sequencing identifies three independent families with biallelic deleterious variants in *COX18*

ES was performed on the affected siblings from family 1. First, we screened for potential pathogenic variants in known CMT genes, but no causal variants were found. Given the reported consanguinity in the family, we then conducted a HOMWES analysis which revealed 17 regions of homozygosity shared between both affected individuals, totaling 33.4Mb in size (the biggest of 8Mb). Variant filtering within those regions and prioritization based on impact and population frequency led to the identification of a homozygous splice variant NM_001297732.2:c.435-6A>G in the second intron of *COX18*. The splice variant was confirmed by Sanger sequencing and analysis of available relatives showed that it co-segregated with the disease (Fig. 1A). The variant was extremely rare in the control population database gnomAD v4.1.0[45], with an allele frequency of 0.00001 and no homozygotes. The variant was predicted by multiple in silico tools (SpliceSiteFinder-like[46], MaxEntScan[47] and NNSPLICE[48]) to abolish the canonical acceptor site in exon 3 and to generate a new acceptor site 6 bp upstream in intron 2 (Fig. 2A). The resulting frameshift was therefore expected to create a premature stop codon in exon 3 and to cause nonsense-mediated decay of *COX18* canonical transcripts (Fig. 2A). Additionally, mtDNA

sequencing showed that the proband from family 1 carried the H1 haplogroup and no pathogenic mtDNA variants.

Screening for additional individuals with *COX18* biallelic deleterious variants in our in-house cohort of 362 unsolved CMT patients (272 with suggestive recessive inheritance and 90 sporadic) did not return any additional affected individuals. However, two additional families were found through the GENESIS[32] and RD-Connect[33] online platforms. Family 2 consisted of four siblings who harbored a homozygous NM_001297732.2:c.215T>G (p.Leu72Arg) (Fig. 1B). The variant is extremely rare (allele frequency of 0.00002, with no homozygotes in gnomAD.[45] Family 3 carried compound heterozygous variants NM_001297732.2:c.328G>C (p.Ala110Pro) and c.893G>C (p.Arg297Pro) which were confirmed to be in trans (Fig.1C). Both variants are exceedingly rare with allele frequencies of 0.000001 and 0.00002, respectively, and had no homozygotes in gnomAD.[45] All these missense variants co-segregated with the disease and were predicted to be deleterious by Polyphen-2 and CADD (CADD PHRED > 20). The mtDNA analysis of the probands from families 2 (2.II.1) and 3 (3.II.1) revealed no pathogenic mtDNA variants and showed they carried the J2a2e and K1a haplogroups, respectively.

All the substitutions affected highly conserved amino acids across different vertebrate species (Fig. 1G). As no crystal structure is available for COX18, AlphaFold[49,50] was used to determine the location and potential impact of the substituted residues. Leu72 lies in a short amphipathic helix (LH1) that faces the inner mitochondrial space, parallel to the inner mitochondrial membrane (Fig.1E and F). The substitution by an arginine introduces a positive charge that might impact the hydrophobic interactions of that helix (Fig. 1F, *left panels*). Ala110 is at the matrix end of the 1st transmembrane helix (TM1) (Fig. 1E and F, *middle panels*) and the introduction of a buried proline in its place is predicted to be structurally damaging by Missense 3D-SB[51,52] (Fig. 1F, *bottom middle panel*). Arg297 residue is located at a loop just after the 5th transmembrane helix (TM5) (Fig. 1E) and shares hydrogen bonds with Ile241 in the 3rd transmembrane domain (Fig. 1G, *top right panel*). The Arg297Pro substitution is predicted by Missense 3D-SB[51,52] to damage the protein structure due to disallowed conformations. Additionally, we hypothesize that the change might abolish the hydrogen bond shared with Ile241, a residue from the 3rd transmembrane helix (TM3) (Fig. 1G, *bottom right*), which might be key for protein folding. This is supported by FoldX[53] in silico tool which estimated that the Arg297Pro could result in a change of protein stability of 3.8kcal/mol.

COX18 deficiency causes a predominant sensory-motor neuropathy phenotype

Detailed clinical features of all eight affected individuals are described in Table 1. The cardinal feature among all patients was progressive sensory-motor axonal polyneuropathy with a variable onset, ranging from 9 to 46 years of age. All patients initially presented with distal lower limb motor and sensory symptoms and, as the disease progressed, most of them slowly developed distal upper limb involvement. Most of the patients presented muscle weakness at disease onset, except for two siblings from family 2, whose phenotypes are predominantly characterized by sensory loss in distal lower limbs. Muscle atrophy was prominent in the feet, in the tibialis anterior and the calf muscles. Two of the patients were dependent on mobility aids, such as a walking stick or wheelchair from middle age. All patients presented sensory loss which followed a stocking and glove pattern. The sense of touch, proprioception, and vibration were impaired, mostly in the lower limbs. One of the individuals (3.II.1) in addition developed, from her mid-thirties, pain in feet and thighs accompanied by a band-like pressure sensation around the legs. Her affected sibling also complained about mild pain until the proximal segment of the calf. All patients suffered from foot deformities, usually in the form of pes cavus, but some of them also presented pes equinovarus and hammer toes. Most of the patients exhibited decreased or absent deep tendon reflexes in distal lower limbs except for the patients from family 3. More specifically, individual 3.II.1 had generalized brisk reflexes except for absent ankle reflexes and as the disease progressed her gait became increasingly spastic and ataxic. Her sister, individual 3.II.2, had a similar presentation with general hyperreflexia and absent ankle reflexes on examination.

Nerve conduction studies (Table 2) revealed decreased compound muscle action potential (CMAP) in peroneal nerve recordings and, in some patients, in the median nerve recordings as well. Sensory nerve action potentials (SNAP) were undetectable in sural nerves in all patients, while ulnar SNAPs were unrecordable in five out of eight of them. Motor nerve conduction velocity (MNCV) was within normal ranges in most patients. Some of the individuals exhibited slightly decreased MNCV which in the context of low amplitudes was attributed to axonal loss. In summary, electrophysiologic studies indicated sensory-motor axonal neuropathy in all the patients.

During the disease course, some patients developed additional symptoms beyond the peripheral nervous system. Affected individuals from family 1 had upper limb tremor and individual 1.II.1 developed cervical dystonia at 45 years of age (Supplementary Video 1), which was treated with botulinum toxin. Patients from family 3 showed brisk deep tendon reflexes and individual 3.II.1 had a particularly complex phenotype characterized by sensory ataxia, spastic gait, and bilateral positive Babinski reflexes. Follow-up studies in this patient revealed mildly elevated serum creatine kinase 165 IU/L (normal range 26-140 IU/L) and brain and spinal MRI revealed mild cerebellar atrophy and cervical spondylosis without myelopathy. Serum lactate in individual 3.II.1 was normal. Her affected sibling 3.II.2 showed a normal brain MRI and spinal MRI showed cervical spondylosis with C5-6 exit foraminal stenosis. Noteworthy, none of the patients presented other mitochondrial-related conditions such as cardiomyopathy, hepatopathy, and tubulopathy.

Splice variant c.435-6A>G leads to alternative splicing resulting in the expression of an aberrant COX18 isoform

To evaluate the impact of the c.435-6A>G variant on splicing, cDNA T-LRS was carried out where we opted to reliably identify potential splicing events triggered by the mutation and quantify all *COX18* transcripts present (Fig. 2A and 2B). To do this, *COX18* cDNA was amplified from EBV-transformed lymphoblasts from the patients, their parents, and unrelated controls. Primers were designed in exon 1 and 4 (Fig. 2A, Supplementary Table 1) to be able to distinguish all previously known and potentially novel *COX18* transcripts and their associated splicing events. Sequencing confirmed that the splice variant generated a new acceptor site in intron 2 that added five coding base pairs to exon 3 (Fig. 2A). The frameshift caused by this insertion generated a premature stop codon in the third exon of the canonical transcripts (Ensembl IDs ENST00000507544.3 and ENST00000295890.8). Accordingly, the mutant canonical transcripts represented a minor portion of the reads in patients and carriers, which suggests that they are most likely degraded by non-sense mediated mRNA decay (NMD) (Fig. 2B). Interestingly, an alternative transcript skipping exon 2 represented as much as 66% of all the transcripts in the patients and 14-27% in the heterozygotes (Fig. 2B). This transcript corresponds to an alternative transcript lacking exon 2 (ENST00000449739.6) that has a

premature stop codon in exon 3 and is normally degraded by NMD. However, instead of being degraded, this transcript recovers its reading frame as a consequence of the splice variant. Canonical wildtype *COX18* transcripts (ENST00000507544.3 and ENST00000295890.8) totaled 86% of the transcripts in unrelated controls and 53-61% in heterozygote carriers (Fig. 2B). In contrast, these canonically spliced transcripts only constituted 4-8% in patients, suggesting that splicing leakage occurs at negligible levels. Another NMD transcript (ENST00000510031.1) with 4bp added to exon 2 was observed in all samples in a minimal proportion, regardless of the genotype (data not shown). The cDNA T-RLS findings were complemented by RT-qPCR experiments using primers located in the exon 5-6 junction and 3'UTR. This way, we quantified the total amount of the longest- and predominant- *COX18* transcripts in all individuals. As expected, the patients expressed lower levels of *COX18* compared to unrelated controls and a similar trend was observed in comparison to the carriers, albeit it was not statistically significant (Supplementary Fig. 1).

Mutant COX18 protein affects the assembly and stability of CIV subunits

COX18 is an assembly factor that translocates the C-terminus of MTCO2, a core subunit of CIV, across the inner mitochondrial membrane (IMM) into the inner mitochondrial space (IMS). Models in yeast and human cells have demonstrated that *COX18* knock-out (KO) impairs MTCO2 insertion across IMM and renders it unstable, ultimately leading to MTCO2 degradation.[54,55] Mutant COX18 protein resulting from the transcript with frame recovery is predicted to be only 4 kDa smaller in molecular mass than the wildtype protein. To evaluate the impact of the splice event on the quantity and function of COX18 and its partner MTCO2, we performed immunoblotting assays with patients' lymphoblasts. Western blotting showed only one protein band corresponding to COX18 in the patients, suggesting that the mutant protein is stably expressed in the patients in comparable amounts to unrelated controls (Fig.2C, Supplementary Fig. 2). However, MTCO2 levels were significantly decreased in patients compared to their heterozygous parents (Fig.2C and D), suggesting that mutant COX18 might affect MTCO2 protein levels. In contrast, unrelated controls showed highly variable expression of MTCO2. We further examined COX18's ability to translocate MTCO2 across the IMM using

a proteinase K (PK) protection assay. The experiment showed that MTCO2 was PK-sensitive and degraded in mitoplasts from the unrelated controls and the carriers, while in the patients' mitoplasts it was protected from degradation (Fig.2E and F). These results point out that mutant COX18 has an impaired ability to insert MTCO2 C-terminus across the IMM, affecting its stability and expression level. To assess the impact of mutant COX18 on the stability of CIV or other complexes, a representative subunit from each complex was immunoblotted (Fig. 2G). The experiment revealed decreased levels of CIV subunit MTCO1, while the subunits from other complexes did not show altered protein levels (Fig. 2H). This suggests that the variant may be associated with an isolated defect in CIV, but further follow-up studies are needed to confirm this.

Splice variant c.435-6A>G impairs CIV activity and mitochondrial membrane potential

Considering that COX18 partial loss of function affects the stability of a core subunit of CIV, we evaluated whether this defect might impact its overall enzymatic activity. CIV is the final enzyme from the electron transport chain. It catalyzes the oxidation of reduced cytochrome c which generates water. This reaction is coupled with the transport of four protons across IMM, contributing to the proton gradient that drives ATP synthesis. To assess the impact of the variant on CIV activity, we performed an enzymatic assay that measures the rate of change in absorbance at 550nm caused by the oxidation of cytochrome c. The assay revealed that patients had a lower CIV to citrate synthetase (CS) enzymatic activity ratio compared to unrelated controls (Fig. 2I). In turn, decreased CIV activity could lead to reduced proton translocation through the IMM. Therefore, mitochondrial membrane potential was measured using flow cytometry on patients' lymphoblasts stained with TMRE, a dye that accumulates in cells with hyperpolarized IMM. TMRE signal was significantly lower in the probands cells compared to carriers and unrelated controls, which indicates a decrease in mitochondrial membrane potential (Fig. 2J).

Drosophila melanogaster COX18 knockdown model displays signs of neurodegeneration

COX18 is a key assembly factor of the mitochondria, and as such, has proven to be functionally conserved from fungi to mammals.[56,57] *COX18* ortholog in *Drosophila melanogaster* (CG4942, dCOX18) shares 61% similarity and 40% identity to the human protein (Supplementary Fig. 3).[58-60] No fly phenotype has been reported to be associated with dCOX18 downregulation. To emulate the partial loss of function of *COX18* observed in the patients, we used a fly line with one copy of dCOX18 disrupted by the insertion of the transposon Minos-mediated integration cassette (MiMIC) within its coding sequence (dCOX18^{MI03165}). Notably, this leads to around 90% reduction of dCOX18 mRNA levels in comparison to naïve flies (yw, Fig. 3B), while pan-neuronal downregulation of dCOX18 expression only led to approximately 75% reduction (Nsyb dCOX18-RNAi, Fig. 3B). Furthermore, when crossing dCOX18^{MI03165} flies to obtain homozygous dCOX18-deficient flies, we observed no offspring, suggesting that the complete loss of dCOX18 in the homozygous null flies is not viable. Therefore, we chose the dCOX18^{MI03165} fly line with severely reduced dCOX18 expression as a biologically relevant model for studying COX18 partial deficiency.

We then assessed whether the dCOX18^{MI03165} flies displayed behavioral and histopathological signs of neurodegeneration. First, we performed a wing degeneration assay to assess if dCOX18 partial loss is associated with axonal degeneration. We evaluated the integrity of the long axons of the chemosensory neurons innervating the wing margin bristles, by expressing a fluorescent red mCherry protein (UAS-mCD8chRFP) in the neuronal membrane (dpr-Gal4 driver) (Fig. 3A). No difference was observed between the fly lines carrying different genotypes on the first day after eclosion. Nonetheless, 30-day-old dCOX18^{MI03165} flies exhibited prominent axonal fragmentation compared to the control fly line (Fig. 3A and C). This degenerative phenotype was comparable to the effect caused by downregulation of Sply, the *Drosophila* ortholog of *SGPL1* that causes axonal CMT in humans.[43] In addition, a negative geotaxis climbing assay was conducted to evaluate the locomotor performance of the dCOX18^{MI03165} flies (Fig. 3D). In this test, the dCOX18^{MI03165} flies presented a slower climbing speed in comparison to the controls (Fig. 3D). The dCOX18^{MI03165} flies climbing performance was similar to the locomotion deficit

presented by another well-established *Drosophila* model, expressing a CMT-causing variant in the *YARS1* gene.[61]

Discussion

This study provides genetic and functional evidence to support *COX18*, a nuclear-encoded mitochondrial assembly factor, as a novel CMT gene candidate. Biallelic missense and splice variants in *COX18* were identified in three families with autosomal recessive axonal CMT. *In-silico* predictions, *in vitro* and *in vivo* studies, suggest that *COX18* partial loss of function is the underlying disease mechanism. Congruently, downregulation of the *COX18* homolog in *Drosophila* replicates key features of neurodegeneration, such as locomotor impairment and axonal degeneration of sensory neurons.

After screening in-house and external CMT cohorts, we have found in total eight patients from three families with biallelic variants in *COX18*. All patients showed sensory-motor axonal polyneuropathy that primarily affects the distal lower limbs. They presented with muscle weakness and atrophy accompanied by foot deformities. The motor impairment significantly affected the ambulation of the patients from families 1 and 2, who were dependent on mobility aids. All individuals experienced sensory loss which was more predominant amongst the affected members from family 3. Electrophysiological studies revealed axonal degeneration of motor and sensory nerves from upper and lower limbs. This is compatible with the literature as the most common type of neuropathy observed in mitochondrial disorders is axonal.[62-64]

Peripheral neuropathy occurs in approximately one-third of the patients with mitochondrial diseases.[65-69] As mitochondrial function is essential for many tissues and systems, mitochondrial peripheral neuropathy usually occurs together with other neurological and extra-neurological manifestations, such as encephalopathy, myopathy, cardiac disease, renal dysfunction.[64,65,67] In some cases, neuropathy can be the only manifestation at onset, but subsequently, other tissues might become affected as the disease progresses.[14,65,70] Likewise, some of the patients reported here developed CNS symptoms during the disease. For instance, patient 1.II.1 developed cervical dystonia in her 40s, three decades after the disease onset. Family 2 seems to be the exception, as all four affected siblings do not show any CNS manifestation. Nevertheless, their peripheral

neuropathy has a late onset (~40s), and it is still plausible that additional symptoms might develop at later stages of the disease.

COX18-related neuropathy showed notable inter- and intra-familial phenotypic variability. Disease onset varied considerably between families, from late childhood to middle adulthood. This clinical heterogeneity might be due to the distinct impact of each variant on COX18 function or the differences in genetic background and epigenetics between the patients. Mitochondria are highly dynamic organelles that can alter their mass, shape, and number to compensate metabolic insults.[71] Moreover, due to the dual genetic origin of mitochondrial proteins, the interaction between nuclear and mtDNA might modulate the penetrance and severity of mitochondrial disease.[72-74] For example, mtDNA variants have been shown to significantly influence the phenotype of mice with pathogenic variants in mitochondrial nDNA genes causing cardiomyopathy.[75] In this study, we did not identify deleterious mtDNA variants that could explain the clinical differences observed, yet the probands from each family carried a different mitochondrial haplogroup which may modify the disease expresion. Finally, environmental modifiers might also play a role in determining the severity and progression of mitochondrial disorders, as observed in mitochondrial optic neuropathies.[76,77]

In this study, we have identified four different *COX18* variants, three missense and one splice variant. All were segregated with the disease in each family and were either novel or extremely rare in public databases. All three missense variants perturbed conserved residues in different domains of the protein. In silico predictions suggest that they are likely deleterious. The p.Ala110Pro and p.Arg297Pro variants are predicted to disrupt the protein structure. While p.Leu72Arg might not affect COX18 structure, it introduces a positive charge in the LH1 amphipathic helix that might affect its function. This domain has been proven to be essential for the insertase function of proteins from the same family (Oxa1/YidC/Alb3) and is thought to destabilize the lipid bilayer and facilitate the release of the inserted protein into the membrane.[78,79] Based on this evidence, these missense variants meet PM2, PP3 and PP1 criteria (variants of unknown significance) from the American College of Medical Genetics and Genomics (ACMG) guidelines.[80] Functional validation of the missense variants is necessary to understand the precise effect of the predicted structural perturbations on COX18 activity.

We studied in detail the functional effect of the splice variant c.435-6A>G. The variant reduces the expression of the canonical transcript to negligible levels, and at the same time, generates an alternatively spliced product missing exon 2. This transcript is the predominant isoform in the patients, while the canonical transcript is marginally expressed. Thus, we attribute the COX18 protein observed in the patients to the expression of a stable but partially functional mutant protein. According to COX18 *in silico* structural models,[49,50] the loss of exon 2 would disrupt a helical hairpin (M1) (Fig.1E) that is well conserved in all translocases from the Oxa1/YidC/Alb3 family.[81] Consistent with our findings, deletions in the same region in the *COX18* ortholog, *yidC*, in *Bacillus subtilis* and *Escherichia coli* do not affect the protein stability but significantly impair its translocase function.[79,82] It is hypothesized that this dynamic and flexible hairpin is in charge of substrate recruitment.[81,83] Likewise, our results highlight the importance of this domain as the aberrant COX18 isoform identified shows a reduced ability to translocate MTCO2 C-terminus, probably owing to difficulties in its recruitment. Thus, based on the evidence provided in this study, the c.435-6A>G variant can be classified as pathogenic according to the ACMG criteria (PS3, PM2, PM4, PP3, PP1).[80]

MTCO2 is a core subunit of CIV which accepts the electrons from cytochrome c through the copper center in its C-terminal and transfers them across the complex to produce water. Patients with the homozygous splice variant showed decreased levels of COX18's substrate MTCO2 compared to their heterozygote parents, who share a similar genetic background. Yet, this difference was not observed when compared to five unrelated controls who showed high interindividual variability in MTCO2 expression in accordance with previous reports[84,85]. Crucially, despite comparable MTCO2 levels to controls, the PK protection assay demonstrated that MTCO2 in patient mitochondria is protected from protease degradation. This indicates that the protein is not properly inserted into the IMM, preventing the C-terminal domain from performing its essential role in electron transfer, and therefore, compromising the function of CIV as a whole. Furthermore, previous studies in *COX18* KO HEK293T cells demonstrated that COX18 translocase activity is necessary for the post-translational stability of MTCO2.[55] The decreased MTCO2 protein levels seen in the patients relative to the parents can therefore be due to this defect in the insertion and folding of MTCO2 which renders it unstable and prone to degradation. The COX18 deficiency observed in the patients was also associated with decreased levels of MTCO1, suggesting a deleterious effect on the stability of another CIV subunit. In turn,

these defects correlated with reduced CIV enzymatic activity and impaired mitochondrial membrane potential. Taken together, we demonstrate that the splice variant affects the chaperone and translocation function of COX18, which ultimately compromises the role of CIV as part of the mitochondrial electron transport chain.

COX18 is expressed in multiple tissues, with the highest expression in EBV-transformed lymphoblasts, adrenal glands, and peripheral nerves.[86] To assess the susceptibility of neurons to *COX18* downregulation in a whole organism, we studied a dCOX18 deficient fly model. The dCOX18^{MI03165} fly displayed signs of neurodegeneration, including age-dependent axonal degeneration of sensory neurons in the wing and locomotor impairment. These results were comparable to the phenotypes observed in previously published CMT fly models, studying mitochondrial or non-mitochondrial CMT-associated genes, which exhibit axonal degeneration and climbing defects as the dCOX18^{MI03165} fly.[16,43,44,87] A similar locomotor impairment has been described in a fly knockdown model of *COA7*, another assembly factor of CIV that has been reported to cause CMT.[16] Additional functional studies on *in vivo* and *in vitro* neuronal models are required to understand the susceptibility of the motor and sensory neurons to the loss of COX18 and to CIV deficiency in general.

A homozygous null *COX18* fly was not possible to obtain, which might suggest that *COX18* complete KO is not viable. While full KO of this gene may be lethal, flies expressing ~10% of COX18 ortholog, were viable and fertile, and demonstrated neurodegenerative phenotypes. Similarly, *COX18*$^{-/-}$ mice exhibit embryonic growth retardation eventually leading to prenatal or preweaning lethality.[88] It is worth noting that some of these mice show abnormalities in the neural tube closure. Altogether, a complete COX18 loss of function seems to be incompatible with life in different species. Therefore, we hypothesize that the variants reported in this study are probably hypomorphic and only partially reduce COX18 function or protein levels.

Despite an earlier study that screened a cohort of patients with CIV deficiency for *COX18* pathogenic variants,[89] the gene had not been linked to any human disease until recently.[24,25] The first report of COX18-related pathology described a patient with neonatal encephalo-cardiomiopathy and CIV deficiency who carried a homozygous NM_001297732.2:c.667G>C p.(Asp223His) variant.[24] Similarly, a recent study reported a COX18 NM_173827.4:c.598G>A(p.Gly200Ser) variant in a patient who developed from 7 months of

age severe and rapidly-progressive motor impairment, resembling spinal muscular atrophy, with dysarthria and oculofacial apraxia.[25] Remarkably, both patients presented axonal peripheral neuropathy as well. Additionaly, an ES study identified through homozygosity mapping *COX18* biallelic variants as a candidate cause for non-syndromic hearing loss, yet functional evaluation was not conducted.[90] Thus, exhaustive phenotyping of additional patients is needed to ascertain the clinical spectrum of COX18-related conditions and further support its role in CMT pathogenesis.

Our findings on COX18-related CMT neuropathy illustrate that in the rare cases where peripheral neuropathy is the main or only clinical feature of an underlying mitochondrial disorder, it is likely to overlook the mitochondrial origin.[65,70] The underlying mitochondrial etiology can be suspected through histochemical, biochemical, and neuroimaging studies. However, no single biomarker is sensitive enough to completely confirm the diagnosis and the lack of abnormal biomarkers does not exclude a mitochondrial dysfunction.[76,91] Similarly, mitochondrial biomarkers, including serum lactate and MRI, did not show consistent findings suggestive of a mitochondrial pathology in our patients. The application of unbiased genetic testing was crucial for establishing the correct etiology. Likewise, using genetic approaches, several studies in the past decade have found different proteins of the mitochondrial respiratory chain to be implicated in the pathogenesis of CMT.[16-22] Thus, our findings, together with these reports, stress the importance of screening mitochondrial genes as part of the diagnostic work-up of patients with CMT with or without a multisystemic clinical presentation.

Among them, biallelic variants in genes encoding subunits or assembly factors of CIV particularly (*SURF1*, *COA7*, *COX6A1,* and *COX20*) have been found to cause CMT.[16-22] Strikingly, some of these genes encode proteins that are also involved in the translocation and maturation of MTCO2. For example, COX20 plays a role as COX18's counterpart by translocating the N-terminus of MTCO2.[20,92,93] SCO2 is a metallochaperone that adds copper to MTCO2's C-terminus once COX18 translocates it into the IMS.[17] What is more, a missense deleterious variant in the mitochondrial gene that encodes MTCO2, COX18's substrate, has been reported to cause late-onset cerebellar ataxia, axonal peripheral neuropathy, and tremor.[94] Interestingly, some of these genes have also been reported to cause severe multisystemic diseases, such as Leigh syndrome (*SURF1*) and cardioencephalomyopathy (*SCO2*).[95,96] These reports, together with the findings of this study, underscore the role of CIV dysfunction in the

pathogenesis of CMT. Further research is needed to understand what makes peripheral neurons particularly susceptible to CIV deficiency and to explain its broad clinical spectrum.

In conclusion, we have provided genetic and functional evidence to support COX18 as a new candidate gene for autosomal recessive axonal CMT. These findings underscore the importance of peripheral neuropathy in the spectrum of mitochondrial disorders, warranting the screening of mitochondrial genes in the diagnostic follow-up of CMT patients with or without CNS features. Our results also recommend the application of next-generation sequencing techniques in the diagnosis of non-syndromic neuropathies of mitochondrial etiology. Moreover, our study provides further evidence to support the critical role of the hairpin domain of COX18 for its translocase activity. Finally, we draw special attention to the impact of mitochondrial CIV deficiency in the pathogenesis of CMT.

Data availability

Experimental data generated during this study can be shared by the corresponding author on reasonable request from any qualified investigator.

Acknowledgements

The authors acknowledge the VIB-UAntwerp Center for Molecular Neurology Neuromics Support Facility for their technical support and Dr. Maria-Luise Petrovic-Erfurth for her feedback during the revision of the manuscript. The authors also thank the patients and their families for participating in this study.

Funding

This work was supported in part by the Fund for Scientific Research (FWO-Flanders) (research grants G048220N and G0A2122N to A.J.; doctoral grants to D.A., L.M., L.VdeV. and S.A.B.), the Research Fund of the University of Antwerp (doctoral grant to C.A.), the Association Belge contre les Maladies Neuromusculaires' (ABMM-Telethon) (research grants to A.J. and S.A.B), the French Muscular Dystrophy Association (AFM-Telethon, research grant 23708 to A.J.,

TRAMPOLINE grant 28730 to S.A.B.). This study makes use of data shared/provided through RD-Connect, which received funding from the European Union Seventh Framework Programme (FP7/2007-2013) under grant agreement No. 305444. This project has received funding from the European Union's Horizon 2020 research and innovation programme under grant agreement No. 779257 (Solve-RD). MMR acknowledges funding from the Medical Research Council (MRC MR/S005021/1), Wellcome Trust (G104817), National Institutes of Neurological Diseases and Stroke and office of Rare Diseases (U54NS065712 and 1UOINS109403-01), Muscular Dystrophy Association (MDA510281), Charcot Marie Tooth Association (CMTA) and the Harrington Discovery Institute. This research was also supported by the National Institute for Health Research University College London Hospitals Biomedical Research Centre.

Competing interests

The authors report no competing interests.

Supplementary material

Supplementary material is available at *Brain* online.

References

1. Barreto LC, Oliveira FS, Nunes PS, et al. Epidemiologic Study of Charcot-Marie-Tooth Disease: A Systematic Review. *Neuroepidemiology.* 2016;46(3):157-165.
2. Pipis M, Rossor AM, Laura M, Reilly MM. Next-generation sequencing in Charcot-Marie-Tooth disease: opportunities and challenges. *Nat Rev Neurol.* 2019;15(11):644-656.
3. Pareyson D, Saveri P, Sagnelli A, Piscosquito G. Mitochondrial dynamics and inherited peripheral nerve diseases. *Neurosci Lett.* 2015;596:66-77.

4. Fridman V, Bundy B, Reilly MM, et al. CMT subtypes and disease burden in patients enrolled in the Inherited Neuropathies Consortium natural history study: a cross-sectional analysis. *J Neurol Neurosurg Psychiatry.* 2015;86(8):873-878.

5. Saporta AS, Sottile SL, Miller LJ, Feely SM, Siskind CE, Shy ME. Charcot-Marie-Tooth disease subtypes and genetic testing strategies. *Ann Neurol.* 2011;69(1):22-33.

6. Abrams AJ, Hufnagel RB, Rebelo A, et al. Mutations in SLC25A46, encoding a UGO1-like protein, cause an optic atrophy spectrum disorder. *Nat Genet.* 2015;47(8):926-932.

7. Manganelli F, Tozza S, Pisciotta C, et al. Charcot-Marie-Tooth disease: frequency of genetic subtypes in a Southern Italy population. *J Peripher Nerv Syst.* 2014;19(4):292-298.

8. Sivera R, Frasquet M, Lupo V, et al. Distribution and genotype-phenotype correlation of GDAP1 mutations in Spain. *Sci Rep.* 2017;7(1):6677.

9. Figueiredo FB, Silva WA, Jr., Giuliatti S, et al. GDAP1 mutations are frequent among Brazilian patients with autosomal recessive axonal Charcot-Marie-Tooth disease. *Neuromuscul Disord.* 2021;31(6):505-511.

10. Auranen M, Ylikallio E, Toppila J, Somer M, Kiuru-Enari S, Tyynismaa H. Dominant GDAP1 founder mutation is a common cause of axonal Charcot-Marie-Tooth disease in Finland. *Neurogenetics.* 2013;14(2):123-132.

11. González-Sánchez P, Satrústegui J, Palau F, Del Arco A. Calcium Deregulation and Mitochondrial Bioenergetics in GDAP1-Related CMT Disease. *Int J Mol Sci.* 2019;20(2).

12. Grel H, Woznica D, Ratajczak K, et al. Mitochondrial Dynamics in Neurodegenerative Diseases: Unraveling the Role of Fusion and Fission Processes. *Int J Mol Sci.* 2023;24(17).

13. Bruhn H, Samuelsson K, Schober FA, et al. Novel Mutation m.10372A>G in MT-ND3 Causing Sensorimotor Axonal Polyneuropathy. *Neurol Genet.* 2021;7(2):e566.

14. Armirola-Ricaurte C, Zonnekein N, Koutsis G, et al. Alternative splicing expands the clinical spectrum of NDUFS6-related mitochondrial disorders. *Genet Med.* 2024;26(6):101117.

15. Baertling F, Sánchez-Caballero L, van den Brand MAM, et al. NDUFA9 point mutations cause a variable mitochondrial complex I assembly defect. *Clin Genet.* 2018;93(1):111-118.

16. Higuchi Y, Okunushi R, Hara T, et al. Mutations in COA7 cause spinocerebellar ataxia with axonal neuropathy. *Brain.* 2018;141(6):1622-1636.

17. Rebelo AP, Saade D, Pereira CV, et al. SCO2 mutations cause early-onset axonal Charcot-Marie-Tooth disease associated with cellular copper deficiency. *Brain.* 2018;141(3):662-672.

18. Echaniz-Laguna A, Ghezzi D, Chassagne M, et al. SURF1 deficiency causes demyelinating Charcot-Marie-Tooth disease. *Neurology.* 2013;81(17):1523-1530.

19. Tamiya G, Makino S, Hayashi M, et al. A mutation of COX6A1 causes a recessive axonal or mixed form of Charcot-Marie-Tooth disease. *Am J Hum Genet.* 2014;95(3):294-300.

20. Xu H, Ji T, Lian Y, et al. Observation of novel COX20 mutations related to autosomal recessive axonal neuropathy and static encephalopathy. *Hum Genet.* 2019;138(7):749-756.

21. Ostergaard E, Weraarpachai W, Ravn K, et al. Mutations in COA3 cause isolated complex IV deficiency associated with neuropathy, exercise intolerance, obesity, and short stature. *J Med Genet.* 2015;52(3):203-207.

22. Kumar R, Corbett MA, Smith NJC, et al. Oligonucleotide correction of an intronic TIMMDC1 variant in cells of patients with severe neurodegenerative disorder. *NPJ Genom Med.* 2022;7(1):9.

23. Pitceathly RD, Murphy SM, Cottenie E, et al. Genetic dysfunction of MT-ATP6 causes axonal Charcot-Marie-Tooth disease. *Neurology.* 2012;79(11):1145-1154.

24. Ronchi D, Garbellini M, Magri F, et al. A biallelic variant in COX18 cause isolated Complex IV deficiency associated with neonatal encephalo-cardio-myopathy and axonal sensory neuropathy. *European Journal of Human Genetics.* 2023;31(12):1414-1420.

25. Mavillard F, Guerra-Castellano A, Guerrero-Gómez D, et al. A splice-altering homozygous variant in COX18 causes severe sensory-motor neuropathy with oculofacial apraxia. *Biochimica et Biophysica Acta (BBA) - Molecular Basis of Disease.* 2024;1870(7):167330.

26. Reumers J, De Rijk P, Zhao H, et al. Optimized filtering reduces the error rate in detecting genomic variants by short-read sequencing. *Nat Biotechnol.* 2011;30(1):61-68.

27. Kancheva D, Atkinson D, De Rijk P, et al. Novel mutations in genes causing hereditary spastic paraplegia and Charcot-Marie-Tooth neuropathy identified by an optimized protocol for homozygosity mapping based on whole-exome sequencing. *Genetics in Medicine.* 2015.

28. Karczewski KJ, Francioli LC, Tiao G, et al. The mutational constraint spectrum quantified from variation in 141,456 humans. *Nature.* 2020;581(7809):434-443.

29. Calabrese C, Simone D, Diroma MA, et al. MToolBox: a highly automated pipeline for heteroplasmy annotation and prioritization analysis of human mitochondrial variants in high-throughput sequencing. *Bioinformatics.* 2014;30(21):3115-3117.

30. Lott MT, Leipzig JN, Derbeneva O, et al. mtDNA Variation and Analysis Using Mitomap and Mitomaster. *Curr Protoc Bioinformatics.* 2013;44(123):1.23.21-26.

31. Schönherr S, Weissensteiner H, Kronenberg F, Forer L. Haplogrep 3 - an interactive haplogroup classification and analysis platform. *Nucleic Acids Research.* 2023;51(W1):W263-W268.

32. Gonzalez M, Falk MJ, Gai X, Postrel R, Schüle R, Zuchner S. Innovative Genomic Collaboration Using the GENESIS (GEM.app) Platform. *Human Mutation.* 2015;36(10):950-956.

33. Lochmüller H, Badowska DM, Thompson R, et al. RD-Connect, NeurOmics and EURenOmics: collaborative European initiative for rare diseases. *European Journal of Human Genetics.* 2018;26(6):778-785.

34. Amor-Barris S, Høyer H, Brauteset LV, et al. HINT1 neuropathy in Norway: clinical, genetic and functional profiling. *Orphanet J Rare Dis.* 2021;16(1):116.

35. Ascari G, Rendtorff ND, De Bruyne M, et al. Long-Read Sequencing to Unravel Complex Structural Variants of CEP78 Leading to Cone-Rod Dystrophy and Hearing Loss. *Front Cell Dev Biol.* 2021;9:664317.

36. Tang AD, Soulette CM, van Baren MJ, et al. Full-length transcript characterization of SF3B1 mutation in chronic lymphocytic leukemia reveals downregulation of retained introns. *Nat Commun.* 2020;11(1):1438.

37. Adriaenssens E, Asselbergh B, Rivera-Mejías P, et al. Small heat shock proteins operate as molecular chaperones in the mitochondrial intermembrane space. *Nature Cell Biology.* 2023;25(3):467-480.

38. Bird MJ, Adant I, Windmolders P, et al. Oxygraphy Versus Enzymology for the Biochemical Diagnosis of Primary Mitochondrial Disease. *Metabolites.* 2019;9(10).

39. Frazier AE, Thorburn DR. Biochemical analyses of the electron transport chain complexes by spectrophotometry. *Methods Mol Biol.* 2012;837:49-62.

40. Schneider CA, Rasband WS, Eliceiri KW. NIH Image to ImageJ: 25 years of image analysis. *Nature Methods.* 2012;9(7):671-675.

41. Storkebaum E, Leitão-Gonçalves R, Godenschwege T, et al. Dominant mutations in the tyrosyl-tRNA synthetase gene recapitulate in Drosophila features of human Charcot–Marie–Tooth neuropathy. *Proceedings of the National Academy of Sciences.* 2009;106(28):11782-11787.

42. Pauli A, Althoff F, Oliveira RA, et al. Cell-type-specific TEV protease cleavage reveals cohesin functions in Drosophila neurons. *Dev Cell.* 2008;14(2):239-251.

43. Atkinson D, Nikodinovic Glumac J, Asselbergh B, et al. Sphingosine 1-phosphate lyase deficiency causes Charcot-Marie-Tooth neuropathy. *Neurology.* 2017:10.1212/WNL.0000.

44. Bervoets S, Wei N, Erfurth M-L, et al. Transcriptional dysregulation by a nucleus-localized aminoacyl-tRNA synthetase associated with Charcot-Marie-Tooth neuropathy. *Nat Commun.* 2019;10(1):5045.

45. Chen S, Francioli LC, Goodrich JK, et al. A genomic mutational constraint map using variation in 76,156 human genomes. *Nature.* 2024;625(7993):92-100.

46. Shapiro MB, Senapathy P. RNA splice junctions of different classes of eukaryotes: sequence statistics and functional implications in gene expression. *Nucleic Acids Res.* 1987;15(17):7155-7174.

47. Yeo G, Burge CB. Maximum entropy modeling of short sequence motifs with applications to RNA splicing signals. *J Comput Biol.* 2004;11(2-3):377-394.

48. Reese MG, Eeckman FH, Kulp D, Haussler D. Improved splice site detection in Genie. *J Comput Biol.* 1997;4(3):311-323.

49. Varadi M, Anyango S, Deshpande M, et al. AlphaFold Protein Structure Database: massively expanding the structural coverage of protein-sequence space with high-accuracy models. *Nucleic Acids Research.* 2021;50(D1):D439-D444.

50. Jumper J, Evans R, Pritzel A, et al. Highly accurate protein structure prediction with AlphaFold. *Nature.* 2021;596(7873):583-589.

51. Ittisoponpisan S, Islam SA, Khanna T, Alhuzimi E, David A, Sternberg MJE. Can Predicted Protein 3D Structures Provide Reliable Insights into whether Missense Variants Are Disease Associated? *Journal of Molecular Biology.* 2019;431(11):2197-2212.

52. Khanna T, Hanna G, Sternberg MJE, David A. Missense3D-DB web catalogue: an atom-based analysis and repository of 4M human protein-coding genetic variants. *Human Genetics.* 2021;140(5):805-812.

53. Schymkowitz J, Borg J, Stricher F, Nys R, Rousseau F, Serrano L. The FoldX web server: an online force field. *Nucleic Acids Res.* 2005;33(Web Server issue):W382-388.

54. Saracco SA, Fox TD. Cox18p is required for export of the mitochondrially encoded Saccharomyces cerevisiae Cox2p C-tail and interacts with Pnt1p and Mss2p in the inner membrane. *Mol Biol Cell.* 2002;13(4):1122-1131.

55. Bourens M, Barrientos A. Human mitochondrial cytochrome c oxidase assembly factor COX18 acts transiently as a membrane insertase within the subunit 2 maturation module. *J Biol Chem.* 2017;292(19):7774-7783.

56. Gaisne M, Bonnefoy N. The COX18 gene, involved in mitochondrial biogenesis, is functionally conserved and tightly regulated in humans and fission yeast. *FEMS Yeast Research.* 2006;6(6):869-882.

57. Funes S, Nargang FE, Neupert W, Herrmann JM. The Oxa2 protein of Neurospora crassa plays a critical role in the biogenesis of cytochrome oxidase and defines a ubiquitous subbranch of the Oxa1/YidC/Alb3 protein family. *Molecular biology of the cell.* 2004;15(4):1853-1861.

58. Hu Y, Flockhart I, Vinayagam A, et al. An integrative approach to ortholog prediction for disease-focused and other functional studies. *BMC Bioinformatics.* 2011;12:357.

59. Neely GG, Hess A, Costigan M, et al. A genome-wide Drosophila screen for heat nociception identifies α2δ3 as an evolutionarily conserved pain gene. *Cell.* 2010;143(4):628-638.

60. Schnorrer F, Schönbauer C, Langer CC, et al. Systematic genetic analysis of muscle morphogenesis and function in Drosophila. *Nature.* 2010;464(7286):287-291.

61. Ermanoska B, Asselbergh B, Morant L, et al. Tyrosyl-tRNA synthetase has a noncanonical function in actin bundling. *Nat Commun.* 2023;14(1):999.

62. Lu JQ, Tarnopolsky MA. Mitochondrial neuropathy and neurogenic features in mitochondrial myopathy. *Mitochondrion.* 2021;56:52-61.

63. Hanna MG, Cudia P. Chapter 84 - Peripheral Nerve Diseases Associated with Mitochondrial Respiratory Chain Dysfunction. In: Dyck PJ, Thomas PK, eds. *Peripheral Neuropathy (Fourth Edition).* Philadelphia: W.B. Saunders; 2005:1937-1949.

64. Bindu PS, Govindaraju C, Sonam K, et al. Peripheral neuropathy in genetically characterized patients with mitochondrial disorders: A study from south India. *Mitochondrion.* 2016;27:1-5.

65. Pareyson D, Piscosquito G, Moroni I, Salsano E, Zeviani M. Peripheral neuropathy in mitochondrial disorders. *Lancet Neurol.* 2013;12(10):1011-1024.

66. Mancuso M, Piazza S, Volpi L, et al. Nerve and muscle involvement in mitochondrial disorders: an electrophysiological study. *Neurol Sci.* 2012;33(2):449-452.

67. Mancuso M, Orsucci D, Angelini C, et al. Mitochondrial neuropathies: A survey from the large cohort of the Italian Network. *Neuromuscul Disord.* 2016;26(4-5):272-276.

68. Finsterer J. Mitochondrial neuropathy. *Clin Neurol Neurosurg.* 2005;107(3):181-186.

69. Colomer J, Iturriaga C, Bestué M, et al. [Aspects of neuropathy in mitochondrial diseases]. *Rev Neurol.* 2000;30(12):1117-1121.

70. Finsterer J. Inherited mitochondrial neuropathies. *Journal of the Neurological Sciences.* 2011;304(1):9-16.

71. Yu SB, Pekkurnaz G. Mechanisms Orchestrating Mitochondrial Dynamics for Energy Homeostasis. *Journal of Molecular Biology.* 2018;430(21):3922-3941.

72. Potluri P, Davila A, Ruiz-Pesini E, et al. A novel NDUFA1 mutation leads to a progressive mitochondrial complex I-specific neurodegenerative disease. *Mol Genet Metab.* 2009;96(4):189-195.

73. Gropman A, Chen TJ, Perng CL, et al. Variable clinical manifestation of homoplasmic G14459A mitochondrial DNA mutation. *Am J Med Genet A.* 2004;124a(4):377-382.

74. Strauss KA, DuBiner L, Simon M, et al. Severity of cardiomyopathy associated with adenine nucleotide translocator-1 deficiency correlates with mtDNA haplogroup. *Proc Natl Acad Sci U S A.* 2013;110(9):3453-3458.

75. McManus MJ, Picard M, Chen HW, et al. Mitochondrial DNA Variation Dictates Expressivity and Progression of Nuclear DNA Mutations Causing Cardiomyopathy. *Cell Metab.* 2019;29(1):78-90.e75.

76. Saneto RP. Mitochondrial diseases: expanding the diagnosis in the era of genetic testing. *J Transl Genet Genom.* 2020;4:384-428.

77. Caporali L, Maresca A, Capristo M, et al. Incomplete penetrance in mitochondrial optic neuropathies. *Mitochondrion.* 2017;36:130-137.

78. Kedrov A, Wickles S, Crevenna AH, et al. Structural Dynamics of the YidC:Ribosome Complex during Membrane Protein Biogenesis. *Cell Rep.* 2016;17(11):2943-2954.

79. Kumazaki K, Chiba S, Takemoto M, et al. Structural basis of Sec-independent membrane protein insertion by YidC. *Nature.* 2014;509(7501):516-520.

80. Richards S, Aziz N, Bale S, et al. Standards and guidelines for the interpretation of sequence variants: a joint consensus recommendation of the American College of Medical Genetics and Genomics and the Association for Molecular Pathology. *Genetics in Medicine.* 2015;17(5):405-423.

81. Hennon SW, Soman R, Zhu L, Dalbey RE. YidC/Alb3/Oxa1 Family of Insertases. *J Biol Chem.* 2015;290(24):14866-14874.

82. Chen Y, Soman R, Shanmugam SK, Kuhn A, Dalbey RE. The role of the strictly conserved positively charged residue differs among the Gram-positive, Gram-negative, and chloroplast YidC homologs. *The Journal of biological chemistry.* 2014;289(51):35656-35667.

83. McDowell MA, Heimes M, Fiorentino F, et al. Structural Basis of Tail-Anchored Membrane Protein Biogenesis by the GET Insertase Complex. *Mol Cell.* 2020;80(1):72-86.e77.

84. Fornetti J, Jindal S, Middleton KA, Borges VF, Schedin P. Physiological COX-2 expression in breast epithelium associates with COX-2 levels in ductal carcinoma in situ and invasive breast cancer in young women. *Am J Pathol.* 2014;184(4):1219-1229.

85. Zidar N, Odar K, Glavac D, Jerse M, Zupanc T, Stajer D. Cyclooxygenase in normal human tissues--is COX-1 really a constitutive isoform, and COX-2 an inducible isoform? *J Cell Mol Med.* 2009;13(9B):3753-3763.

86. Consortium G. The Genotype-Tissue Expression (GTEx) project. *Nat Genet.* 2013;45(6):580-585.

87. Ermanoska B, Motley WW, Leitão-Gonçalves R, et al. CMT-associated mutations in glycyl- and tyrosyl-tRNA synthetases exhibit similar pattern of toxicity and share common genetic modifiers in Drosophila. *Neurobiology of Disease.* 2014;68:180-189.

88. Bult CJ, Blake JA, Smith CL, Kadin JA, Richardson JE. Mouse Genome Database (MGD) 2019. *Nucleic Acids Res.* 2019;47(D1):D801-d806.

89. Sacconi S, Salviati L, Trevisson E. Mutation analysis of COX18 in 29 patients with isolated cytochrome c oxidase deficiency. *Journal of Human Genetics.* 2009;54(7):419-421.

90. Mohseni M, Babanejad M, Booth KT, et al. Exome sequencing utility in defining the genetic landscape of hearing loss and novel-gene discovery in Iran. *Clin Genet.* 2021;100(1):59-78.

91. Hubens WHG, Vallbona-Garcia A, de Coo IFM, et al. Blood biomarkers for assessment of mitochondrial dysfunction: An expert review. *Mitochondrion.* 2022;62:187-204.

92. Otero MG, Tiongson E, Diaz F, et al. Novel pathogenic COX20 variants causing dysarthria, ataxia, and sensory neuropathy. *Ann Clin Transl Neurol.* 2019;6(1):154-160.

93. Dong HL, Ma Y, Yu H, et al. Bi-allelic loss of function variants in COX20 gene cause autosomal recessive sensory neuronopathy. *Brain.* 2021;144(8):2457-2470.

94. Zierz CM, Baty K, Blakely EL, et al. A Novel Pathogenic Variant in MT-CO2 Causes an Isolated Mitochondrial Complex IV Deficiency and Late-Onset Cerebellar Ataxia. *J Clin Med.* 2019;8(6).

95. Papadopoulou LC, Sue CM, Davidson MM, et al. Fatal infantile cardioencephalomyopathy with COX deficiency and mutations in SCO2, a COX assembly gene. *Nat Genet.* 1999;23(3):333-337.

96. Lee IC, El-Hattab AW, Wang J, et al. SURF1-associated Leigh syndrome: a case series and novel mutations. *Hum Mutat.* 2012;33(8):1192-1200.

Figure legends

Figure 1 Biallelic variants in *COX18* in three families with autosomal recessive axonal CMT. (**A-C**) Pedigree and variant segregation of the Families 1-3. Squares indicate males and circles represent females. Black symbols indicate affected individuals. Arrows point at the proband of each family. Asterisks specify the patients whose exome was sequenced. The diagonal line across a symbol denotes a deceased individual. (**D**) Distribution of the variants on the *COX18* gene. (**E**) Diagram of COX18 domains (top left), predicted protein structure model of COX18 (top right) and distribution of the variants on the COX18 protein (bottom). (**F**) The position of the residues affected by the missense variants is shown within COX18's predicted 3D protein structure. Original amino acids (green) are indicated by black arrowheads (top panels), while mutated residues (red) are indicated by red arrowheads (bottom panels).(**G**) Amino acid

conservation of the Leu72, Ala110, and Arg297 residue across multiple species. IMS = intermembrane space; IMM: inner mitochondrial membrane; MTS: mitochondrial targeting sequence; LH: amphipathic helix; TM: transmembrane helix; M1: hairpin-like domain.

Figure 2 Functional characterization of COX18:c.435-6A>G variant in patients' EBV-transformed lymphoblasts. (**A**) Exon-intron architecture of wildtype *COX18* transcripts. Splicing junctions are depicted as carets connecting the exons, junctions of the canonical transcripts (ENST00000507544.3, ENST00000295890.8) are colored in blue and the junction of the exon 2 skip transcript (ENST00000449739.6) is shown in purple. Orange arrows represent the forward and reverse primers used for *COX18* cDNA T-LRS. The effect of the variant on splicing is shown inside a dialog box underneath exon 3. Diagrams of the wildtype transcripts and the abnormally spliced transcripts that result from the splice variant are shown in the right panel. (**B**) Relative quantification of *COX18* transcripts sequenced by cDNA T-LRS in homozygous (hmz), heterozygous (htz), and control individuals shows that the mutant transcript skipping exon 2 is the predominant transcript in the homozygous patients (n = 1 for each genotype, with 2 biological replicates for each genotype). (**C** and **D**) Immunoblotting of full lysate protein from EBV-transformed lymphoblasts derived from the individuals with different genotypes shows no reduced levels of COX18. Please note that mutant COX18 protein, resulting from the transcript with frame recovery, is predicted to be only 4 kDa smaller than wildtype COX18, making the two isoforms indistinguishable from each other on the blot. Western blot analysis revealed reduced levels of MTCO2 in the homozygotes compared to the carrier but not to five unrelated controls. Data are shown as mean ± SD (n = 3). (**E** and **F**) Proteinase K (PK) protection assay in mitoplasts from lymphoblasts of the homozygous proband indicates that MTCO2 is protected from degradation, while heterozygotes and unrelated controls show increased levels of degraded MTCO2. The levels of degraded MTCO2 (deg. MTCO2) relative to the levels of intact MTCO2 in the untreated mitochondrial fraction are shown as mean ± SD (n = 3 for each genotype, 2 biological replicates were tested for the homozygous genotype). SDHA is a mitochondrial matrix protein and HCCS is an inner mitochondrial (IMM) protein. (**G** and **H**) Western blot of mitochondrial fractions from lymphoblasts revealed decreased protein levels of complex IV (CIV) subunit MTCO1 in the homozygotes relative to unrelated controls and heterozygotes. The asterisk indicates an unspecific band. Immunoblotting quantification of

MTCO1 is shown as mean ± SD (n = 3 for each genotype, with 2 biological replicates for each genotype). (**I**) Normalized CIV to citrate synthetase (CS) activity is decreased in homozygotes compared to the other genotypes. Values are shown as mean ± SD (n = 3). (**J**) Flow cytometry analysis of mitochondrial membrane potential with TMRE staining shows decreased median fluorescence intensity (MFI) in lymphoblasts from homozygous patients relative to unrelated controls. ****P<0.0001, ***P<0.001, **P<0.01, *P<0.05, ns: not significant.

Figure 3 Downregulation of *COX18*'s ortholog in Drosophila, dCOX18, causes age-dependent axonal degeneration of sensory neurons and locomotor impairment. (**A**) The nerve tract along the L1 wing vein was visualized by mCherry expression using dpr-Gal4 driver. Representative images are shown from 1-day and 30-day-old flies from each genotype. RNAi Sply flies were used as positive control. Flies expressing the driver alone were used as negative control. (**B**) Quantification of dCOX18 RNA expression using RT-qPCR for control (yw), Nsyb-driven RNAi dCOX18 pan-neuronal knockdown (Nsyb-Gal4 > dCOX18-RNAi), and dCOX18^{MI03165} fly lines. Data are shown as mean ± SD (n=2). (**C**) Quantification of the percentage of wings with axonal fragmentation at day 30. (n = 23-48 per genotype). (**D**) Climbing performance of control (yw), dCOX18^{MI03165}, and YARS1-E196K fly lines was assessed by measuring the climbing time of 10-day-old flies. Data are shown as mean ± SD (n = 15-25, 10 groups of 10 flies tested for each phenotype). ***P<0.001, **P<0.01, *P<0.05, ns: not significant.

Table 1 Clinical features of the index patients

General features	Family 1		Family 2				Family 3	
	II.1	II.2	II.1	II.2	II.3	II.4	II.1	II.2
Ethnicity/Consanguinity	Serbian/Yes		Egyptian/No				British/No	
Sex/AOO (y)	F/~10	M/~10	M/40	M/46	M/28	M/30	F/9	F/14
Symptoms at onset	Weakness and wasting in DLL	Weakness and wasting in DLL	Numbness, weakness and wasting in DLL	Numbness, weakness and wasting in DLL	Intermittent numbness in DLL	DLL numbness, slipper slippage while walking	High feet arches, running difficulties	Ankle sprains and falls
Age at last exam. (y)	51	35	50	54	32	44	44	50
Main symptoms	Severe weakness in DLL and mild in DUL	Severe weakness in DLL and mild in DUL	Numbness, weakness in DLL and DUL	Weakness and numbness in DLL	Numbness, weakness and wasting in DLL	Weakness and wasting in DLL	Weakness in DLL and DUL, numbness in DLL	Weakness in DLL and DUL, numbness in DLL, ankle instability
Mobility	Wheelchair, walking stick from age 40y	Independent	Independent	Independent	Independent	Independent	Spastic gait, independent	Walking stick from age 40y
Clinical diagnosis	CMT2	CMT2	CMT2	CMT2	CMT2	CMT2	CMT2 with UMN signs	CMT2 with hyperreflexia
Pyramidal and PNS								
Strength DLL/DUL	0-1/3-4	0-1/5	0/4	0/4	2/5	1-2/5	1/4	0/3-4
Atrophy DLL/DUL[a]	++/+	++/+	++/+	++/+	++/+	++/+	++/+	++/-
Abnormal deep tendon reflexes	Achilles absent	Achilles absent	Achilles absent	Achilles absent	Achilles ↓	Achilles ↓	All ↑, Achilles ↓	All ↑, Achilles absent
Plantar responses[b]	Mute	Mute	Mute	Mute	Mute	Mute	Extensor	Mute
Foot deformities	Pes cavus equinovarus	Pes cavus	Pes cavus, hammer toes	Pes cavus, hammer toes	Pes cavus, hammer toes	Pes cavus, hammer toes	High arches	Bilateral foot triple arthrodesis in 20s
Sensory								
Touch deficit	+	+	+	+	+	+	NT	NT
Propioception/vibration deficit	+	+	+	+	+	+	+	+
Pain/temperature deficit	NT	NT	+	+	+	+	+	+
Neuropathic pain	-	-	-	-	-	-	Moderate	Mild
Brain MRI	Normal	-	-	-	-	-	Mild cerebellar atrophy	Normal
Other	Cervical dystonia; postural tremor of DUL; depression	Postural tremor of DUL.		T2DM			Spasticity; sensory ataxia; Spinal MRI: mild cervical spondylosis; mildly elevated serum CK; normal serum lactate	Spinal MRI: cervical spondylosis with C5-6 exit foraminal stenosis; T2DM

AOO = Age of onset; DLL = distal lower limbs; DUL = distal upper limbs; CMT2 = Axonal Charcot-Marie-Tooth disease; UMN = upper motor neuron; PNS = peripheral nervous system; ↓ = reduced; ↑ = brisk; NT = not tested; T2DM = diabetes mellitus type 2; CK = creatine kinase.
[a]Muscle atrophy is reported as moderate (++), mild (+) or absent (-).

[b]Bilateral plantar responses are reported.

Table 2 Electrophysiological studies of the index patients

Nerve	NCS	Family 1		Family 2				Family 3	
		II.1	II.2	II.1	II.2	II.3	II.4	II.1	II.2
Median	CMAP (mV)	5.8	3.3	0.83	0.25	6.5	0.35	7.6	6.4
	MNCV (m/s)	47.7	55.9	50	36	58.2	30.0	55	48
Peroneal	CMAP (mV)	ND	ND	ND	0.45	4.53	ND	1.2	0.8
	MNCV (m/s)				24.0	40.6		44	28
Ulnar	SNAP (μV)	23.2	NP	20.8	ND	30.5	ND	ND	ND
	SNCV (m/s)	40.0		28.6		26.8			
Sural	SNAP (μV)	ND	ND	ND	ND	ND	ND	ND	ND
	SNCV (m/s)								
Electrophysiological diagnosis		Sensory-motor axonal CMT	Sensory-motor axonal CMT	Sensory-motor axonal CMT	Sensory-motor axonal CMT	Sensory-motor axonal CMT	Sensory-motor axonal CMT	Sensory-motor axonal CMT	Sensory-motor axonal CMT

NCS: nerve conduction studies; CMAP: compound muscle action potential; MNCV: motor nerve conduction velocity; SNAP: sensory nerve action potential; SNCV: sensory nerve conduction velocity; ND: not detected; NP: not performed; CMT: Charcot-Marie-Tooth disease; NA: not applicable.

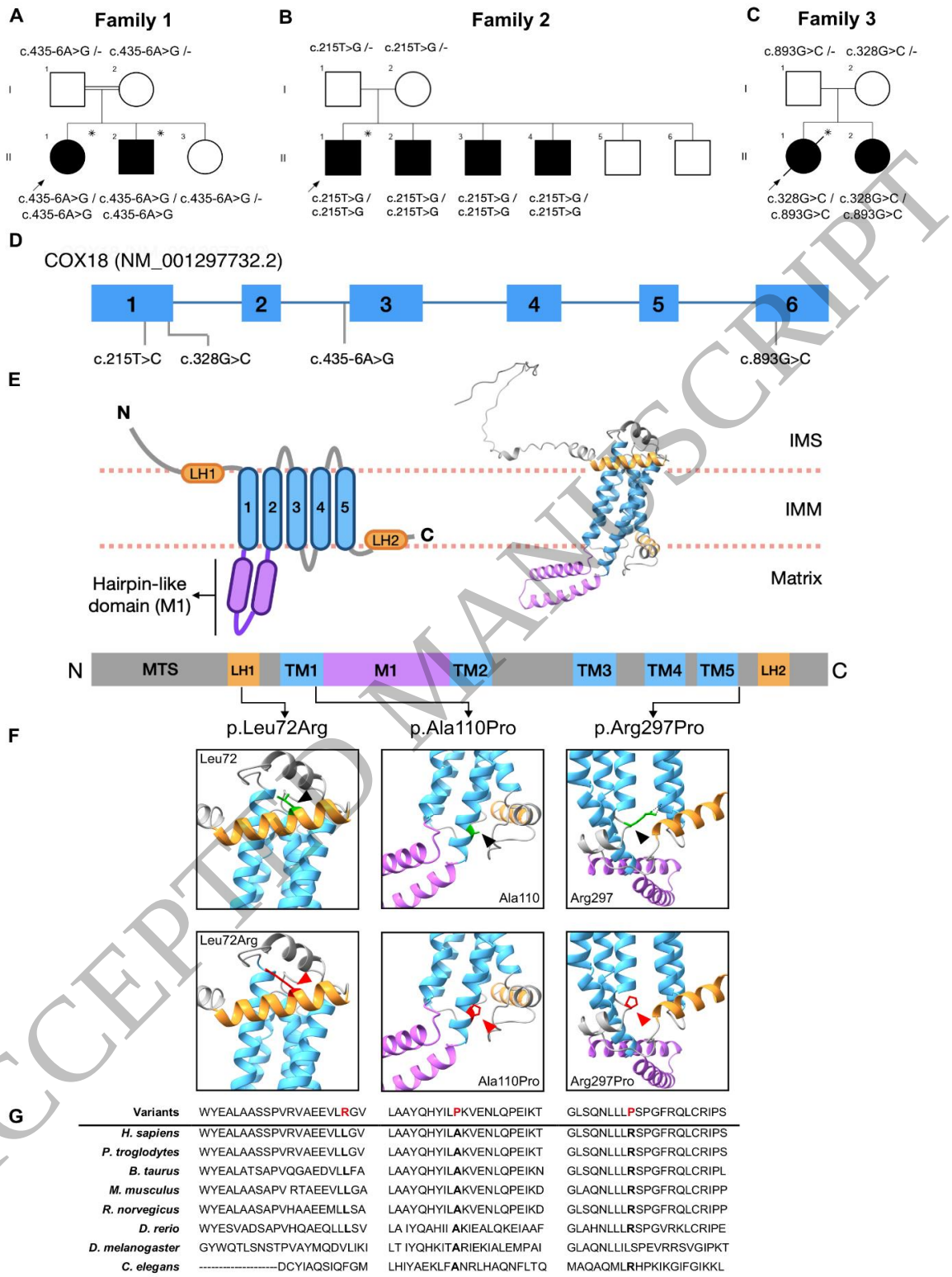

Figure 1
159x224 mm (x DPI)

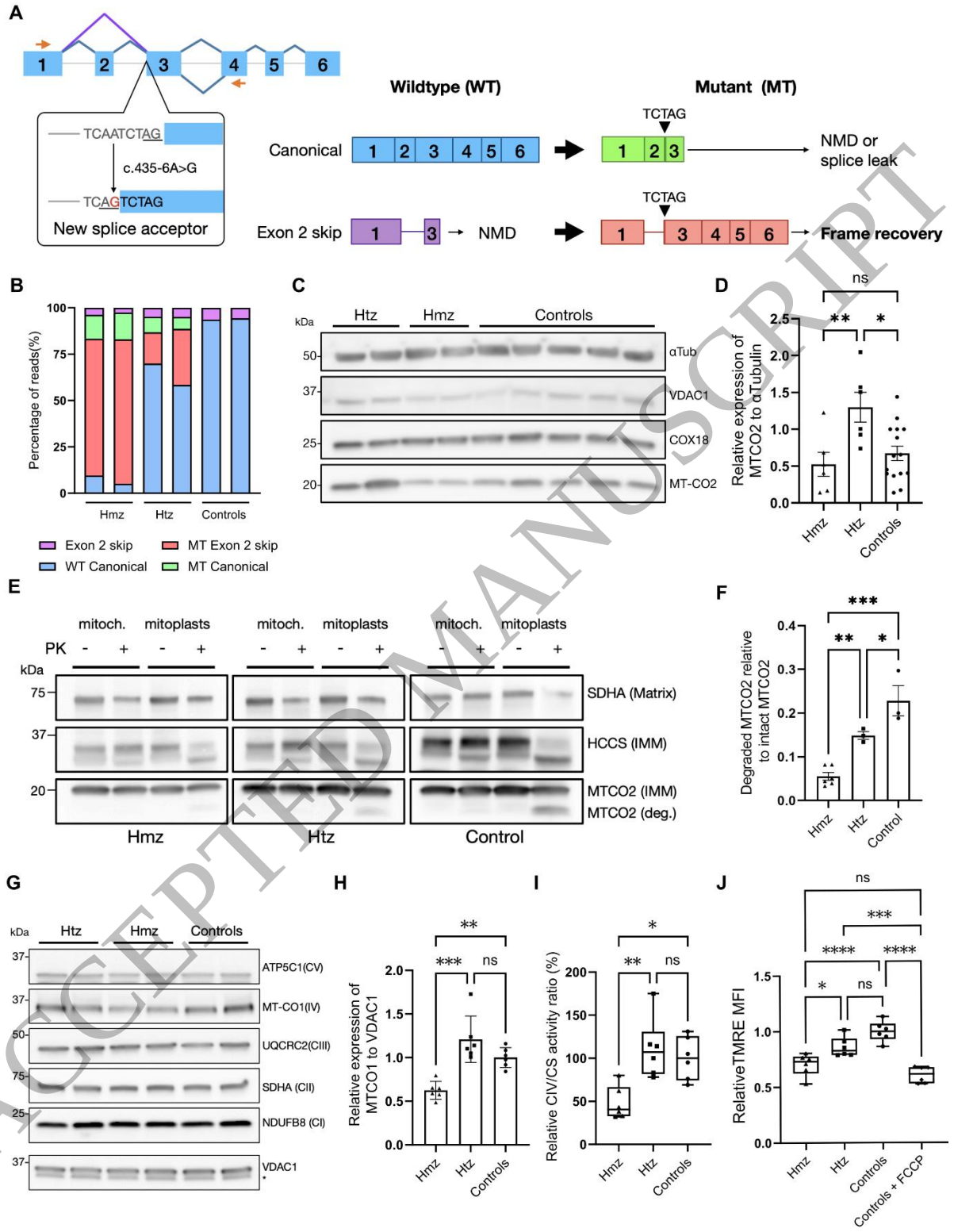

Figure 2
159x207 mm (x DPI)

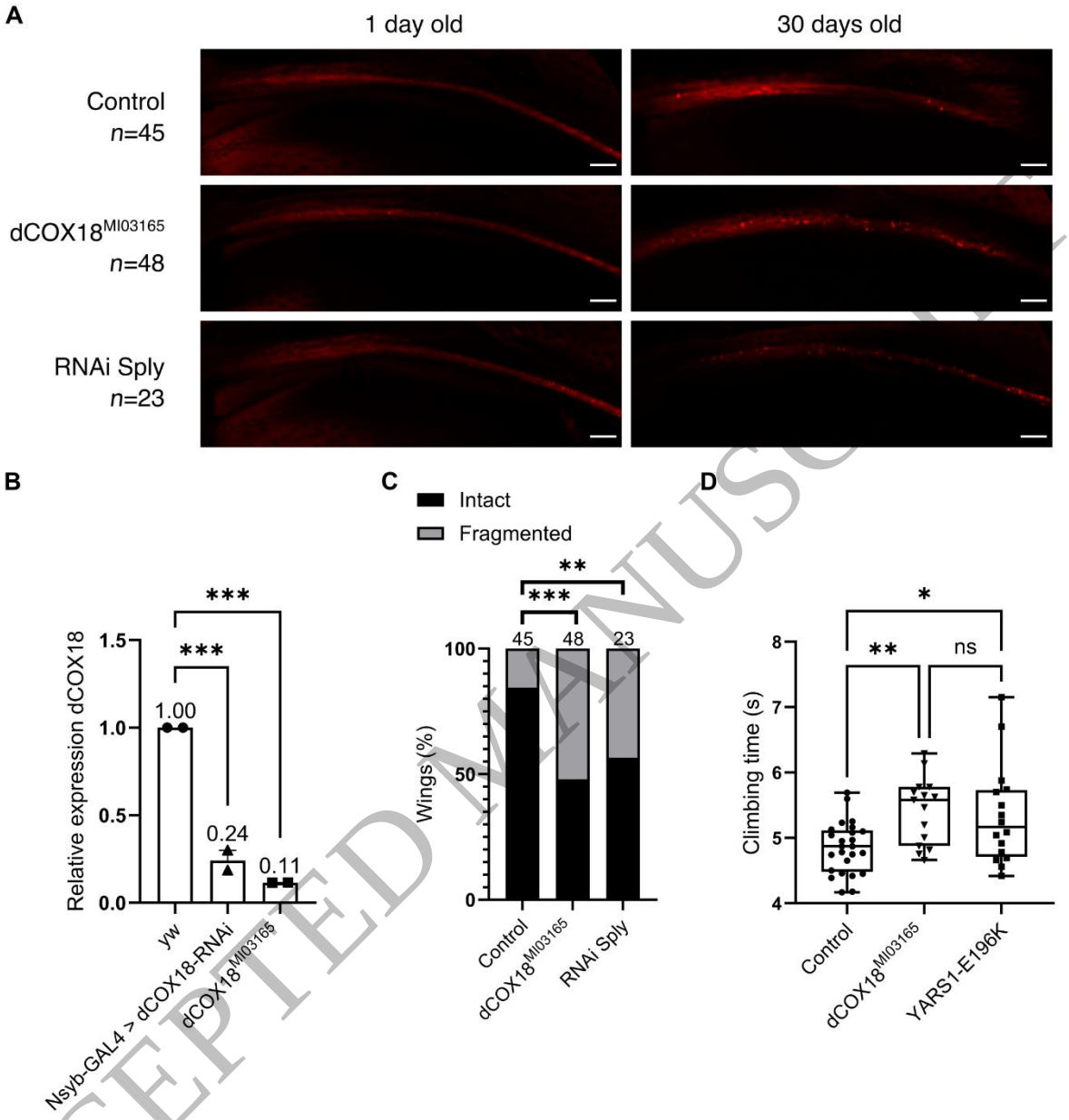

Figure 3
159x164 mm (x DPI)

TYSABRI™ (natalizumab)
SUBCUTANEOUS USE | 300mg

This promotional article is authored and funded by Biogen.
This material is intended for UK and IE healthcare professionals only.

Prescribing Information

Efficacy made Convenient

TYSABRI SC injection with the potential to administer **AT HOME** for eligible patients*

Efficacy and safety profile comparable between TYSABRI IV and SC†[1,2]

†Comparable PK, PD, efficacy, and safety profile of SC to IV except for injection site pain.[1,2]

CLICK HERE TO DISCOVER MORE ABOUT TYSABRI SC AND THE DIFFERENCE IT MAY MAKE TO YOUR ELIGIBLE PATIENTS

Supported by

BIOGEN'S Stratify JCV™ SERVICE

A Biogen developed and funded JCV antibody index PML risk stratification service, validated and available exclusively for patients on or considering TYSABRI.

*As of April 2024, TYSABRI SC can be administered outside a clinical setting (e.g. at home) by a HCP for patients who have tolerated at least 6 doses of TYSABRI well in a clinical setting. Please refer to section 4.2 of the SmPC.[1]

TYSABRI is indicated as single DMT in adults with highly active RRMS for the following patient groups:[1,2]

- **Patients with highly active disease despite a full and adequate course of treatment with at least one DMT**
- **Patients with rapidly evolving severe RRMS defined by 2 or more disabling relapses in one year, and with 1 or more Gd+ lesions on brain MRI or a significant increase in T2 lesion load as compared to a previous recent MRI**

Very common AEs include nasopharyngitis and urinary tract infection. Please refer to the SmPC for further safety information, including the risk of the uncommon but serious AE, PML.[1,2]

Abbreviations: AE: Adverse Event; **DMT:** Disease-Modifying Therapy; **Gd+:** Gadolinium-Enhancing; **HCP:** Healthcare Professional; **IV:** Intravenous; **JCV:** John Cunningham Virus; **MRI:** Magnetic Resonance Imaging; **PD:** Pharmacodynamic; **PK:** Pharmacokinetic; **PML:** Progressive Multifocal Leukoencephalopathy; **RRMS:** Relapsing-Remitting Multiple Sclerosis; **SC:** Subcutaneous.

References: 1. TYSABRI SC (natalizumab) Summary of Product Characteristics. **2.** TYSABRI IV (natalizumab) Summary of Product Characteristics.

Adverse events should be reported. For Ireland, reporting forms and information can be found at www.hpra.ie. For the UK, reporting forms and information can be found at https://yellowcard.mhra.gov.uk/ or via the Yellow Card app available from the Apple App Store or Google Play Store. Adverse events should also be reported to Biogen Idec on MedInfoUKI@biogen.com 1800 812 719 in Ireland and 0800 008 7401 in the UK.

Biogen-261128. DOP: April 2025

Biogen